



Verification of image quality improvement by deep learning reconstruction to 1.5 T MRI in T2-weighted images of the prostate gland

Yoshiomi Sato¹ · Kiyoshi Ohkuma²

Received: 19 March 2024 / Revised: 16 May 2024 / Accepted: 4 June 2024 / Published online: 8 June 2024

© The Author(s), under exclusive licence to Japanese Society of Radiological Technology and Japan Society of Medical Physics 2024

Abstract

This study aimed to evaluate whether the image quality of 1.5 T magnetic resonance imaging (MRI) of the prostate is equal to or higher than that of 3 T MRI by applying deep learning reconstruction (DLR). To objectively analyze the images from the 13 healthy volunteers, we measured the signal-to-noise ratio (SNR) and contrast-to-noise ratio (CNR) of the images obtained by the 1.5 T scanner with and without DLR, as well as for images obtained by the 3 T scanner. In the subjective, T2W images of the prostate were visually evaluated by two board-certified radiologists. The SNRs and CNRs in 1.5 T images with DLR were higher than that in 3 T images. Subjective image scores were better for 1.5 T images with DLR than 3 T images. The use of the DLR technique in 1.5 T MRI substantially improved the SNR and image quality of T2W images of the prostate gland, as compared to 3 T MRI.

Keywords Magnetic resonance imaging · Deep learning reconstruction · Prostate gland · T2-weighted image · Image quality

1 Introduction

Prostate cancer (PCa) is the second most commonly diagnosed cancer and the fifth leading cause of cancer death among men worldwide, with an estimated 1,400,000 new PCa cases and 375,000 deaths in 2020 [1]. Additionally, the incidence of PCa is increasing in most Asian countries [2]. PCa is expected to become more prevalent in an aging population [3]. Magnetic resonance imaging (MRI) is widely used as a non-invasive tool for the assessment of PCa, because its high resolution provides images with excellent anatomical features and soft tissue high contrast. Currently, the magnetic field strengths of MRI scanners used in medicine are mainly the 3 T and 1.5 T MRI. Previous studies have reported that 3 T MRI scanners are clinically useful for imaging the prostate gland [4, 5]. Another study

reported that the 3 T MRI scanner has made detailed assessment of the prostate gland anatomy possible, thus improving the precision of diagnosis [6]. Since high-resolution images are required for detailed evaluation of the prostate gland anatomy, the Prostate Imaging Reporting and Data System (PI-RADS) version 2.1 guidelines recommend the use of 3 T-MRI scanners [7].

The signal-to-noise ratio (SNR) of the 3 T MRI scanner is channeled into increasing the quality, resolution, or various combinations of these effects of MRI images [8]. The 1.5 T MRI scanner has a lower magnetic field strength than the 3 T MRI scanner; therefore, its spatial resolution is lower with a larger image noise [9]. However, the 1.5 T MRI scanner has advantages over the 3 T MRI scanner, in terms of the effects of magnetic susceptibility artifacts on prostate diffusion-weighted magnetic resonance imaging (DW-MRI) [10] and B1 inhomogeneities, as well as inspection costs and safety [11, 12]. Additionally, MRI using lower static magnetic fields is safer for patients with metal implants. As a result, 1.5 T MRI scanners are widely used. Previous studies comparing the T2W images of the prostate produced by the 3 T and 1.5 T MRI scanners have indicated that T2WI images of the prostate gland are capable of providing equivalent diagnoses, regardless of the magnetic field strengths

✉ Yoshiomi Sato
yoshiomi@msh.biglobe.ne.jp

¹ Department of Radiology, Saitama City Hospital, Mimuro 2460, Saitama 336-8522, Japan

² Department of Diagnostic Radiology, Saitama City Hospital, Mimuro 2460, Saitama 336-8522, Japan

[13]. However, regarding the T2WI imaging parameters in the previous study, the T2W images of the prostate produced by the 1.5 T-MRI scanner had a larger image pixel size than those by the 3 T-MRI scanner. Additionally, the SNR was ensured by increasing the number of excitations. As the spatial resolution of images is increased, the available signal per voxel decreases, leading to a reduced SNR. Therefore, to obtain an SNR with a 1.5 T-MRI scanner equivalent to that with a 3 T-MRI scanner, adjustments, such as reduction in in-plane resolution and extension of scan time, may be needed due to an increase in the number of excitations.

In recent years, due to the advanced application of artificial intelligence (AI) to medicine, the emergence of the deep learning reconstruction (DLR) technology has attracted much attention as a new SNR improvement technology for MRI images. DLR has been introduced by few MR vendors to improve the quality of MRI images, and it has been widely reported for its clinical usefulness [14–20]. In this same period, the Canon Medical Systems Corporation developed a deep learning-based denoising technique, which is currently commercially available as Advanced intelligent Clear IQ Engine (AiCE), in MRI scanners [21].

The denoising approach with DLR, developed using soft shrink convolutional neural networks (SCNN), is a technique that can reduce image noise and reconstruct high SNR images from low SNR images [21].

Some clinical studies reported the clinical usefulness of DLR in imaging not only the central nervous system but also other body systems [21–29]. Those studies have shown that using a similar protocol, the 1.5 T scanner with DLR images can achieve lesser noise and higher overall image quality than the 3 T scanner [27–29].

We hypothesized that using a 1.5 T MRI scanner with DLR could provide a similar image quality of the prostate as that obtained with a 3 T MRI without DLR. Therefore, this study sought to compare image quality of T2-weighted MRI images of the prostate gland between the 1.5 T scanner with DLR and 3 T scanner without DLR.

2 Materials and methods

2.1 Image acquisition

The images used in this study were T2W images obtained by 1.5 T and 3 T MRI scanners (Vantage Oriion and Vantage Galan 3 T, Canon Medical Systems, Tochigi, Japan) with Atlas SPEEDER Body coil and Atlas SPEEDER Spine coil. The scan parameters were fast spin echo sequence, TR:4000 ms, TE:120 ms, number of acquisitions: 2, echo train length:19, pixel bandwidth: 279 Hz, FOV:18×18 cm, 256×256 pixels (0.7 mm/pixel), slice thickness: 2 mm, slice gap: 0.2 mm, NAQ:2, SPEEDER:2, Scan time: 3:30 s. The

study included 13 healthy volunteers (23–57 years old [mean age of 38.6 ± 11.6 years]), and all images were produced with the same T2W scan parameters. The T2W prostate image scan parameters were based on the PI-RADS™ v2.1 settings, incorporating high-resolution scan parameters. Thereafter, we assessed for differences in image quality of T2W images of the prostate between the 1.5 T scanner with DLR and the 3.0 T scanner and verified the possibility of producing images with similar image qualities by both scanners. In this study, the sequence of two scans on 1.5 T and 3 T scanners was randomized and we attempted to minimize the interval between the two scans.

2.2 Image analysis

To objectively analyze the images from the healthy volunteers, we measured the SNR and contrast-to-noise ratio (CNR) of the images obtained by the 1.5 T scanner with and without DLR, as well as for images obtained by the 3 T scanner.

The identical region of interest (ROI) method was used to measure the SNR. To quantitatively evaluate images, a board-certified radiological technologist with MRI expertise performed ROI measurements. ROIs were placed over the prostate peripheral zone (PZ), transition zone (TZ), and obturator muscle of each volunteer (Fig. 1). The approximate area of the ROI in the PZ, TZ, and obturator muscle was 20 mm². The ROI in the PZ was positioned as centrally as possible within the right side. The ROI in the TZ was placed within the low signal area of the left TZ as much as possible. The ROI in the obturator muscle was positioned

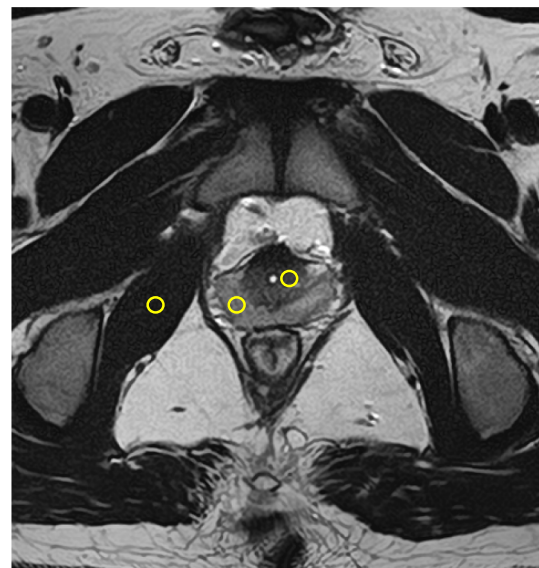


Fig. 1 Regions of interest at the prostate peripheral zone, transition zone, and obturator muscle levels in the axial sectional image

as centrally as possible within the right obturator muscle near the prostate. The ROIs were placed manually, which might have caused measurement errors; however, each ROI was positioned in exactly the same way for the three different types of images, to reduce the possibility of significant measurement error. For quantitative image indexes, SNR and CNR were calculated using the following:

$$\text{SNR} = \frac{\text{SI}_{\text{tissue(a)}}}{\text{SD}_{\text{tissue(a)}}},$$

$$\text{CNR} = \frac{\text{SI}_{\text{tissue(a)}} - \text{SI}_{\text{tissue(b)}}}{\text{SD}_{\text{tissue(a)}}},$$

where SI tissue (a), (b) is the average signal intensity of tissue in the ROI, and SD tissue (a) is the average standard deviation of tissue in the ROI.

In the subjective analysis of healthy volunteers, T2W images of the prostate were visually evaluated by two board-certified radiologists. The evaluators were blinded to the field strength and identity of the volunteers and asked to rate the images by consensus on a five-point scale. All images obtained with the acquisition protocols for 1.5 T and 3.0 T MRI were scored for visualization of the anatomic structures (prostate capsule, boundary between the transition and the peripheral zones, seminal vesicle, and obturator muscle), noise, artifact, and overall image quality. The scoring criteria are shown in Table 1. Subjective image scores were ranked as described previously [27]. The visibility of the anatomic structures was ranked as follows: 1—not visible, 2—mostly not visible or blurred, 3—mostly visible but partially blurred, 4—subtle blurring, and 5—homogeneous internal intensity with sharp edge. The indicator of image noise was ranked as

follows: 1—unacceptable noise, 2—strong noise but still diagnostic, 3—acceptable noise, 4—minimal noise, and 5—no noise. The indicator of image artifact was ranked as follows: 1—unacceptable artifact, 2—strong artifact but still diagnostic, 3—acceptable artifact, 4—minimal artifact, and 5—no artifact. The indicator of overall image quality was ranked as follows: 1—unacceptable, 2—average, 3—fair, 4—very good, and 5—excellent.

2.3 Statistical analysis

To compare objective image quality indexes, SNR and CNR for 1.5 T without DLR, 1.5 T with DLR, and 3 T without DLR were reported as means \pm standard deviation and compared using the Tukey HSD test. Subjective image analysis indexes were reported as medians and interquartile ranges (IQR) and compared using the Friedman test with Bonferroni correction. We used nonparametric tests, because ordinal data from subjective evaluations are non-normally distributed. And we used the Friedman test to compare the image quality yielded by 1.5 T, 1.5 T with DLR, and 3 T MRI in the same volunteers in this study. We conducted our study in accordance with the cited literature, wherein Akai et al. used the Friedman test in the same way to compare the 1.5 T, 1.5 T with DLR, and 3 T MRI. A p -value < 0.05 was considered to indicate statistical significance. Inter-observer variability between the readers was measured using Cohen's weighted kappa coefficient. The kappa values were considered as follows: poor, 0.00–0.20; fair, 0.21–0.40; moderate, 0.41–0.60; good, 0.61–0.80; and excellent, 0.81–1.00 [30]. All statistical analyses were performed using a free statistical software, EZR version 1.55 (Saitama Medical Center, Jichi Medical University, Saitama, Japan) [31].

Table 1 Scoring of criteria used for visual evaluation of prostate images

| Score | Visibility of prostate capsule | Visibility of the boundary between the transition and the peripheral zones | Visibility of seminal vesicle | Visibility of obturator muscle | Image noise | Image artifact | Overall image quality |
|-------|--|--|--|--|-----------------------------------|--------------------------------------|-----------------------|
| 1 | Not visible | Not visible | Not visible | Not visible | Unacceptable noise | Unacceptable artifact | Unacceptable |
| 2 | Mostly not visible or blurred | Mostly not visible or blurred | Mostly not visible or blurred | Mostly not visible or blurred | Strong noise but still diagnostic | Strong artifact but still diagnostic | Average |
| 3 | Mostly visible but partially blurred | Mostly visible but partially blurred | Mostly visible but partially blurred | Mostly visible but partially blurred | Acceptable noise | Acceptable artifact | Fair |
| 4 | Subtle blurring | Subtle blurring | Subtle blurring | Subtle blurring | Minimal noise | Minimal artifact | Very good |
| 5 | Homogeneous internal intensity with sharp edge | Homogeneous internal intensity with sharp edge | Homogeneous internal intensity with sharp edge | Homogeneous internal intensity with sharp edge | No noise | No artifact | Excellent |

2.4 Denoising approach with deep learning-based reconstruction: DLR

In this study, we used a deep learning-based denoising technique, which is currently commercially available as Advanced intelligent Clear IQ Engine (AiCE) [21]. AiCE is a DLR that uses deep convolutional neural networks (CNNs), and more information on CNNs can be found in previous literature [21]. DLR can reduce image noise by learning various noise characteristics using different noise level images and ground-truth images [21]. Figure 2 illustrates the architecture of the CNN. The CNN of the DLR consists of three layers: the feature extraction, feature conversion, and image generation layer. The feature extraction layer is convolved with 7×7 discrete-cosine-transform (DCT) convolution to divide into a zero-frequency component path and high frequency component path and high frequency component path.

High frequency components derived by DCT convolution components undergo repeated 3×3 convolution and soft shrinkage in the feature conversion layers. Finally, in the image generation layer, the denoised output image is generated by deconvolution with a 7×7 inverse DCT kernel followed by addition of the segmented zero-frequency. The zero-frequency component path adapts the image generation layer without adapting the next feature transformation layer. Therefore, image contrast can be maintained. Because low SNRs in medical images can interfere with diagnostic imaging and image analysis, medical image denoising procedures with high contrast are of clinical importance. Medical images should be free of noise for correct diagnosis. T2WI is essential to evaluate anatomical details in the prostate gland, and the prostate images with improved SNR and CNR using DLR may be useful in clinical practice.

3 Results

Representative volunteer images are shown in Fig. 3.

3.1 Objective analysis

Figure 4 shows the results for SNR and CNR measurements of the three methods.

In the PZ of the prostate, the SNR of the 1.5 T images with DLR (9.02 ± 1.74) was higher than that of the 1.5 T images without DLR (4.47 ± 1.20) and 3 T images (6.25 ± 1.23) ($P < 0.05$).

In the TZ, the SNR of the 1.5 T images with DLR (4.73 ± 0.94) was higher than that of the 1.5 T images without DLR (2.31 ± 0.47) and 3 T images (3.44 ± 0.84) ($P < 0.05$). In the obturator muscle, the SNR of the 1.5 T images with DLR (2.67 ± 0.41) was significantly higher than that of the 1.5 T images without DLR (1.60 ± 0.16) and 3 T images (1.65 ± 0.17) ($P < 0.05$). However, no difference in SNR was observed between the 1.5 T images without DLR and 3 T images ($P = 0.87$).

The CNR of the TZ and PZ of the prostate was 4.85 ± 1.83 on 1.5 T images with DLR, which was higher than that on 1.5 T images without DLR (2.35 ± 1.27) and 3 T images (3.02 ± 1.53) ($P < 0.05$). However, no difference in CNR was observed between 1.5 T images without DLR and 3 T images ($P = 0.55$). The CNR of the PZ and obturator muscle was 7.57 ± 1.71 on 1.5 T images with DLR, which was higher than that on 1.5 T images without DLR (3.49 ± 1.19) and 3 T images (5.32 ± 1.23) ($P < 0.05$). The CNR of the TZ and obturator muscle was 3.03 ± 0.97 on 1.5 T images with DLR, was higher than that on 1.5 T (1.22 ± 0.44) and 3 T

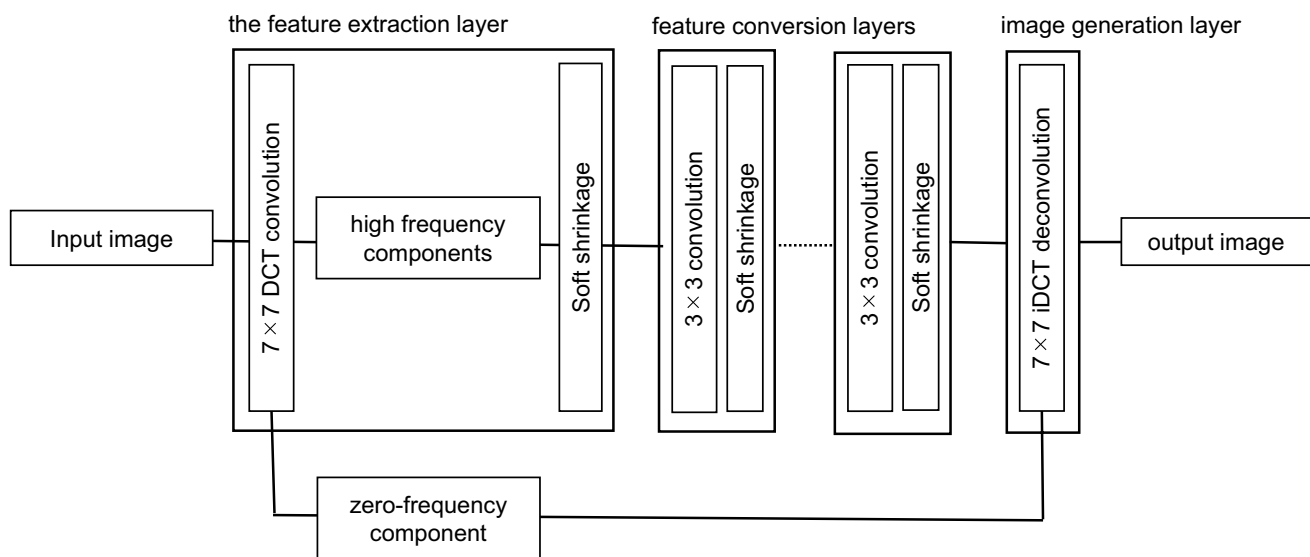


Fig. 2 The schematic of architecture of the denoising procedure with deep learning-based reconstruction (DLR) algorithm

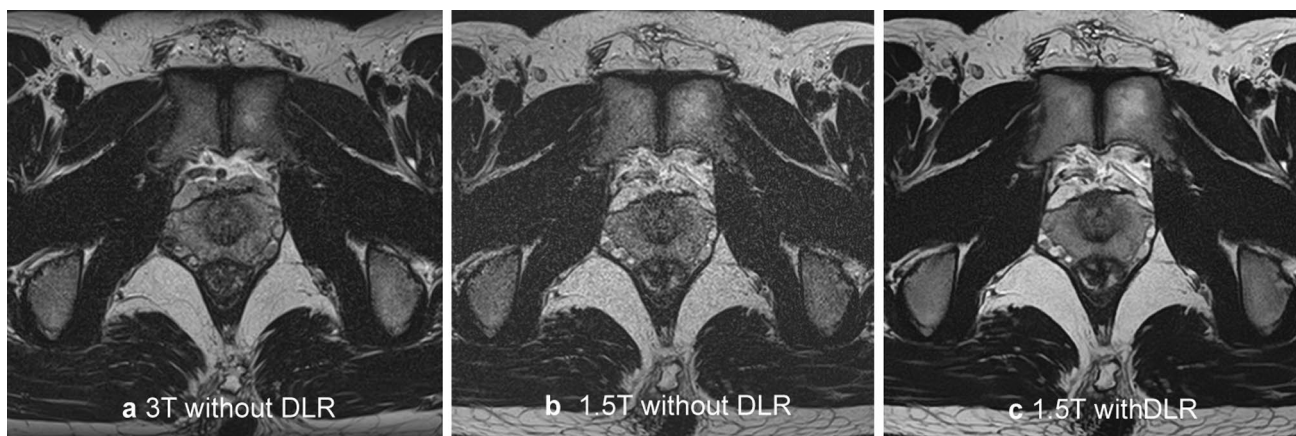


Fig. 3 Representative prostate images from a healthy volunteer: **a** 3 T without DLR, **b** 1.5 T without DLR, **c** 1.5 T with DLR

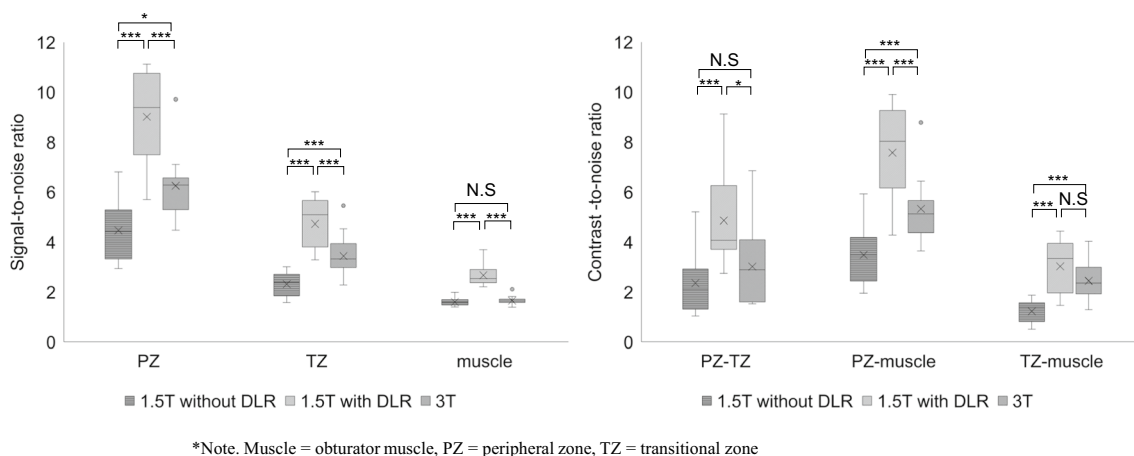


Fig. 4 Results of comparison of each quantitative image quality index among the three methods

(2.44 ± 0.73) images without DLR. However, no difference in CNR was observed between 1.5 T images with DLR and 3 T images ($P=0.14$).

3.2 Subjective analysis

The results of all subjective analyses are shown in Table 2. All scores for visibility of the anatomic structures on 1.5 T images with DLR were significantly higher than those on 1.5 T images without DLR and 3 T images for both readers. The scores of artifacts on 1.5 T images with DLR were comparable to those of the 1.5 T images without DLR and 3 T images for the two readers, without any significant difference. Scores of image noise and overall image quality of 1.5 T images with DLR were significantly higher than those of 1.5 T images without DLR and 3 T images for both readers.

The inter-reader agreement between both readers, as measured by Cohen's kappa, was excellent for visibility of anatomic structures (prostate capsule: 0.755, boundary between TZ and PZ: 0.784, obturator muscle: 0.794, and seminal vesicle: 0.829). Additionally, the agreement for artifacts was moderate (0.595), whereas that for noise (0.936) and overall image quality (0.894) were excellent. We provided clear detailed explanations to the observers about the definitions of the evaluation criteria and classification methods for the images to minimize the variability between the two observers.

4 Discussion

PI-RADS version 2.1 recommends the use of 3 T-MRI scanners, because diagnosis of lesions of small anatomical structures, such as the prostate, high spatial resolution

Table 2 Results of subjective image analyses

| Reader | Results of qualitative analysis | | | | | | |
|---|---------------------------------|-------------------|---------|-----------------------|-------------------------------------|--------------------------|-------|
| | Measured value | | | p-value | | k-value | |
| | 1.5 T with DLR | 1.5 T without DLR | 3 T | 1.5 T with DLR vs 3 T | 1.5 T with DLR vs 1.5 T without DLR | 1.5 T without DLR vs 3 T | |
| <i>Prostate capsule</i> | | | | | | | |
| Reader1 | 5 (5–5) | 2 (2–3) | 3 (3–3) | 0.002 | 0.004 | 0.372 | 0.755 |
| Reader2 | 5 (4–5) | 2 (2–2) | 3 (3–3) | 0.021 | 0.006 | 0.006 | |
| <i>The boundary between the transition and the peripheral zones</i> | | | | | | | |
| Reader1 | 5 (3–5) | 1 (1–1) | 2 (2–3) | 0.016 | 0.016 | 0.021 | 0.784 |
| Reader2 | 3 (3–5) | 2 (1–2) | 3 (2–3) | 0.022 | 0.004 | 0.006 | |
| <i>Seminal vesicle</i> | | | | | | | |
| Reader1 | 5 (5–5) | 2 (2–2) | 4 (2–4) | 0.007 | 0.003 | 0.04 | 0.829 |
| Reader2 | 5 (4–5) | 2 (2–3) | 3 (2–4) | 0.014 | 0.004 | 0.11 | |
| <i>Obturator muscle</i> | | | | | | | |
| Reader1 | 5 (5–5) | 3 (3–3) | 4 (3–4) | 0.003 | 0.003 | 0.018 | 0.794 |
| Reader2 | 5 (5–5) | 3 (3–4) | 4 (4–4) | 0.003 | 0.004 | 0.035 | |
| <i>Noise</i> | | | | | | | |
| Reader1 | 5 (5–5) | 1 (1–1) | 2 (2–3) | 0.004 | 0.001 | 0.004 | 0.936 |
| Reader2 | 5 (5–5) | 1 (1–1) | 3 (3–3) | 0.003 | 0.004 | 0.004 | |
| <i>Artifact</i> | | | | | | | |
| Reader1 | 5 (5–5) | 5 (5–5) | 5 (2–5) | 0.27 | 1 | 0.27 | 0.595 |
| Reader2 | 5 (5–5) | 4 (4–5) | 4 (3–5) | 0.085 | 0.079 | 0.39 | |
| <i>Overall image quality</i> | | | | | | | |
| Reader1 | 5 (5–5) | 1 (1–1) | 3 (3–3) | 0.003 | 0.003 | 0.006 | 0.894 |
| Reader2 | 5 (4–5) | 1 (1–1) | 3 (3–3) | 0.003 | 0.003 | 0.002 | |

*Statistically significant difference ($P < 0.05$)

images with high SNR are required. Generally, 3 T MRI scanners can produce higher SNR than 1.5 T scanners. However, 3 T MRI scanners with high static magnetic fields are not widely used in clinical practice as 1.5 T MRI scanners. In addition, in regard to metallic implants, Jennifer Jerrolds and Shane Keene [11] stated that one of the most important safety concerns in the MRI environment is the effect of the magnetic field on medical devices and implants. He also stated that just as some supporting equipment is not transferrable from 1.5 to 3 T, some medical devices that are safe in 1.5 T scanners are not safe to use in 3 T scanners. Therefore, High static magnetic fields, as 3 T scanners, may increase risk in patients with metal implants.

Our results showed that T2W images of the prostate produced by 1.5 T scanners with DLR had better image noise than those by 3 T scanners. Image quality of the 1.5 T scanner with DLR was significantly higher than that of the 3 T scanner. First, prostate 1.5 T images with DLR were quantitatively evaluated in comparison to 1.5 T images without DLR and 3 T images. The SNRs of the PZ, TZ, and obturator muscle of each volunteer in 1.5 T images with DLR were significantly higher than those in 3 T images.

The CNR of 1.5 T images with DLR was higher than that of 3 T images. However, the standard deviation of all measured CNRs was large, and the CNR of the TZ and obturator muscle was not statistically significant. One possible reason is the inter-individual differences. In our study, data were obtained from 13 healthy volunteers (ages: 23–57 years [mean age of 38.6 ± 11.6 years]). Regarding age-related changes of the normal prostate, Zhang [32] stated that the internal structures of the prostate constantly change due to aging and alterations in sex hormone. Additionally, previous studies have demonstrated a significant relationship between age and T2W image intensity of the TZ [33]. From these studies, we confirmed the variation in measurement among volunteers.

Thereafter, 1.5 T images with DLR, 1.5 T without images, and 3 T images were assessed subjectively by two board-certified radiologists for visibility of the anatomic structures, image noise, artifacts, and overall image quality. Our findings indicated that, for the scoring of the visual evaluation of visibility of anatomic structures, image noise, and overall image quality, the 3 T images were significantly superior to the 1.5 T images without DLR. These results show that 3 T scanners produce images with a higher SNR than 1.5 T

scanners, which is consistent with reports recommending 3 T scanners, such as the PI-RADS.

The anatomical visibility, image noise, and overall image quality scores for 1.5 T images with DLR were significantly higher than those for 1.5 T images without DLR and 3 T images. No significant difference in artifact scores were observed. Therefore, 1.5 T scanners with DLR improves the image quality of original images and generates images that are almost equivalent or even superior to 3 T MRI images. In this study, images processed with DLR were compared with those processed without the use of DLR. However, if images processed with DLR were compared with histopathology images or high-quality images obtained with longer scan times, more accurate results could be obtained.

To the best of our knowledge, our study is the first to compare 1.5 T with DLR images and 1.5 T and 3 T images without DLR from the same volunteers using same scan parameters by MRI units. Additionally, our study used a slice thickness of 2 mm, which exceeds PI-RADS's recommended thin slice thickness for high-resolution images. With a 2-mm slice thickness, imaging of the prostate structure is likely to improve due to reduction in partial-volume averaging.

According to PI-RADS, T2W images can be used to identify the anatomy of prostatic zones and evaluate abnormalities within the prostate gland. Therefore, T2W images are considered crucial for diagnosis of prostate lesions. From our results, the use of 1.5 T scanners with DLR can improve image quality and potentially produce images comparable to 3 T images, which is considered highly beneficial in clinical practice. If, for some reason, a patient cannot undergo MRI examination in a 3 T scanner, it is clinically very useful to be able to safely perform the examination in a 1.5 T scanner with DLR to obtain images that meet the recommended criteria of PIRADS.

This study had several limitations. First, all study participants were healthy volunteers, and no participants had prostate lesions. Therefore, evaluation of prostate lesions by the 1.5 T MRI with DLR technique remains unknown. Further studies in a larger group of patients with various prostate lesions would be needed to fully validate the DLR technology. Second, we assessed the utility of DLR for only T2W imaging but not the DWI or DCE imaging, because T2W imaging is key for diagnosing prostate lesions. Further studies are needed to investigate the effects on other sequences. Third, the imaging locations were not identical between the 1.5 T and 3 T MRI images, which may have affected the visualization of anatomic structures. However, we attempted to minimize the interval between the two scans. Fourth, we tested the utility of 1.5 T with DLR for only TZ of the prostate, PZ of the prostate, and obturator muscle, and not for other organs in this study. Although deep learning reconstruction primarily removes Gaussian

noise, the 1.5 T with DLR images sometimes gave different impressions of internal structures from the 3 T images, especially the linear sub-structures within the adipose tissue. In general, higher DLR settings tend to make images excessively smooth, and the optimal DLR setting may depend on the parameters employed on the 1.5 T system. Therefore, without appropriate DLR settings, the visibility of small structures may be reduced in images obtained using DLR. The extent of such denoising was not quantified in our study and requires further investigation. Fifth, to avoid selection bias, we recruited volunteers consecutively in this study, which may have resulted in a wide age range of volunteers, which, in turn, could have resulted in relatively wide variations in the prostate anatomy and signal properties, affecting the SNR and CNR measurements. In future studies, subjects should be stratified into equal-sized groups by age, to determine if findings similar to those in this study could be obtained in any age group. Sixth, we did not conduct a comparative study of the image quality obtained with 3 T with DLR and 1.5 T with DLR MRI of the prostate in this study. Since DLR has already been applied successfully to 3 T MRI of other areas such as brain, heart, and female pelvis [21, 23], it is likely to provide equally good images of the prostate. In this study, however, we did not evaluate the image quality obtained with addition of DLR to 3 T MRI, because this study was primarily aimed at determining if the addition of DLR to 1.5 T MRI might provide image quality equal to or better than that obtained with the 3 T MRI as recommended in the PI-RADS version 2.1 guidelines. Future comparisons of 1.5 T with DLR and 3 T with DLR MRI will provide a clearer perspective of the impact of DLR applied to MRI at different field strengths. Considering these issues, further investigations on the application of the DLR technique in routine clinical examination are warranted. We consider that the six items mentioned in the limitation section are issues that need validation in future studies. Future investigations addressing these issues would be expected to provide a clearer perspective of the usefulness of application of DLR to 1.5 T MRI.

5 Conclusion

The use of the DLR technique in 1.5 T MRI substantially improved the SNR and image quality of T2W images of the prostate gland, as compared to 3 T MRI. The clinical benefit of using DLR with 1.5 T MR images of the prostate should be investigated in future studies of real patients; however, the results of the present preliminary study conducted in healthy volunteers are valuable. Our study results have significant clinical implications for institutions and patients who do not have access to 3 T MRI facilities.

Data availability statement The data used to support the findings of this study are available from the corresponding author on reasonable request.

Declarations

Conflict of interest The author declares no conflict of interest.

Ethics approval This study was conducted with the approval of the ethics committee of the facility to which the author belongs. The images used in this study were deidentified and anonymized to protect the personal information of participants.

References

- Sung H, Ferlay J, Siegel RL, et al. Global cancer statistics 2020: GLOBOCAN estimates of incidence and mortality worldwide for 36 cancers in 185 countries. *CA Cancer J Clin*. 2021;71:209–49. <https://doi.org/10.3322/caac.21660>.
- Kimura T, Egawa S. Epidemiology of prostate cancer in Asian countries. *Int J Urol*. 2018;25:524–31. <https://doi.org/10.1111/iju.13593>.
- Jeremy YCT, Hoyee WH, Jason MWH, et al. Global incidence of prostate cancer in developing and developed countries with changing age structures. *PLoS ONE*. 2019;14(10):e0221775. <https://doi.org/10.1371/journal.pone.0221775>.
- Kaji Y, Kuroda K, Maeda T, Kitamura Y, Fujiwara T, Matsuoka Y, Tamura M, Takei N, Matsuda T, Sugimura K. Anatomical and metabolic assessment of prostate using a 3-Tesla MR scanner with a custom-made external transceive coil: healthy volunteer study. *J Magn Reson Imaging*. 2007;25(3):517–26. <https://doi.org/10.1002/jmri.20829>.
- Park JJ, Kim CK, Park SY, Park BK, Lee HM, Cho SW. Prostate cancer: role of pretreatment multiparametric 3-T MRI in predicting biochemical recurrence after radical prostatectomy. *Am J Roentgenol*. 2014;202:W459–65. <https://doi.org/10.2214/ajr.13.11381>.
- Sklinda K, Fraczek M, Mruk B, et al. Normal 3T MR anatomy of the prostate gland and surrounding structures. *Adv Med*. 2019;2019:3040859. <https://doi.org/10.1155/2019/3040859>.
- PI-RADS (2019) Prostate imaging reporting and data system version 2.1. *Am Coll Radiol*
- Mara MB, Smith MP, Pedrosa I, et al. Body MR imaging at 3.0 T: understanding the opportunities and challenges. *Radiographics*. 2007;27:1445–62. <https://doi.org/10.1148/rg.275065204>.
- Isoda H, Kataoka M, Maetani Y, et al. MRCP imaging at 3.0 T vs 1.5 T: preliminary experience in healthy volunteers. *J Magn Reson Imaging*. 2007;25:1000–6. <https://doi.org/10.1002/jmri.20892>.
- Mazaheri Y, Vargas HA, Nyman G, Akin O, Hricak H, et al. Image artifacts on prostate diffusion-weighted magnetic resonance imaging: trade-offs at 1.5 Tesla and 3.0 Tesla. *Acad Radiol*. 2013;20:1041–7. <https://doi.org/10.1016/j.acra.2013.04.005>.
- Jerrolds J, Keene S. MRI safety at 3 T versus 1.5 T. *Internet J World Health Soc Polit*. 2009;6(1).
- Greenman RL, Shirofsky JE, Mulkern RV, Rofsky NM. Double inversion black-blood fast spin-echo imaging of the human heart: a comparison between 1.5 T and 3.0 T. *J Magn Reson Imaging*. 2003;17:648–55. <https://doi.org/10.1002/jmri.10316>.
- Ullrich T, Quentin M, Oelers C, et al. Magnetic resonance imaging of the prostate at 1.5 versus 3.0 T: a prospective comparison study of image quality. *Eur J Radiol*. 2017;90:192–7. <https://doi.org/10.1016/j.ejrad.2017.02.044>.
- Yokota Y, Takeda C, Kidoh M, et al. Effects of deep learning reconstruction technique in high-resolution non-contrast magnetic resonance coronary angiography at a 3-tesla machine. *Can Assoc Radiol J*. 2021;72:120–7. <https://doi.org/10.1177/0846537119900469>.
- Akatsuka J, Yamamoto Y, Sekine T, et al. Illuminating clues of cancer buried in prostate MR image: deep learning and expert approaches. *Biomolecules*. 2019;9:673. <https://doi.org/10.3390/biom9110673>.
- Qiu D, Zhang S, Liu Y, et al. Super-resolution reconstruction of knee magnetic resonance imaging based on deep learning. *Comput Methods Prog Biomed*. 2020;187: 105059. <https://doi.org/10.1016/j.cmpb.2019.105059>.
- Lee KL, Kessler DA, Dezonie S, et al. Assessment of deep learning-based reconstruction on T2-weighted and diffusion-weighted prostate MRI image quality. *Eur J Radiol*. 2023;166: 111017. <https://doi.org/10.1016/j.ejrad.2023.111017>.
- Kim EH, Choi MH, Lee YJ, et al. Deep learning-accelerated T2-weighted imaging of the prostate: Impact of further acceleration with lower spatial resolution on image quality. *Eur J Radiol*. 2021;145: 110012. <https://doi.org/10.1016/j.ejrad.2021.110012>.
- Wang X, Ma J, Bhosale P, et al. Novel deep learning-based noise reduction technique for prostate magnetic resonance imaging. *Abdom Radiol*. 2021;46:3378–86. <https://doi.org/10.1007/s00261-021-02964-6>.
- Gassenmaier S, Afat S, Nickel MD, et al. Accelerated T2-weighted TSE imaging of the prostate using deep learning image reconstruction: a prospective comparison with standard T2-weighted TSE imaging. *Cancers*. 2021;13:3593. <https://doi.org/10.3390/cancers13143593>.
- Kidoh M, Shinoda K, Kitajima M, et al. Deep learning based noise reduction for brain MR imaging: tests on phantoms and healthy volunteers. *Magn Reson Med Sci*. 2020;19(3):195–206. <https://doi.org/10.2463/mrms.mp.2019-0018>.
- Yasaka K, Akai H, Sugawara H, et al. Impact of deep learning reconstruction on intracranial 1.5 T magnetic resonance angiography. *Jpn J Radiol*. 2022;40(5):476–83. <https://doi.org/10.1007/s11604-021-01225-2>.
- Ueda T, Ohno Y, Yamamoto K, et al. Compressed sensing and deep learning reconstruction for women's pelvic MRI denoising: utility for improving image quality and examination time in routine clinical practice. *Eur J Radiol*. 2021;134: 109430. <https://doi.org/10.1016/j.ejrad.2020.109430>.
- Tajima T, Akai H, Sugawara H, et al. Breath-hold 3D magnetic resonance cholangiopancreatography at 1.5 T using a deep learning-based noise-reduction approach: comparison with the conventional respiratory-triggered technique. *Eur J Radiol*. 2021;144:109994. <https://doi.org/10.1016/j.ejrad.2021.109994>.
- Tanabe M, Higashi M, Yonezawa T, et al. Feasibility of high-resolution magnetic resonance imaging of the liver using deep learning reconstruction based on the deep learning denoising technique. *Magn Reson Imaging*. 2021;80:121–6. <https://doi.org/10.1016/j.mri.2021.05.001>.
- Ueda T, Ohno Y, Yamamoto K, et al. Deep learning reconstruction of diffusion-weighted MRI improves image quality for prostatic imaging. *Radiology*. 2022;303:373–81. <https://doi.org/10.1148/radiol.204097>.
- Akai H, Yasaka K, Sugawara H, et al. Commercially available deep-learning-reconstruction of MR imaging of the knee at 1.5T has higher image quality than conventionally-reconstructed imaging at 3T: a normal volunteer study. *Magn Reson Med Sci*. 2023;22:353–60. <https://doi.org/10.2463/mrms.mp.2022-0020>.
- Yasaka K, Tanishima T, Ohtake Y, et al. Deep learning reconstruction for the evaluation of neuroforaminal stenosis using 1.5T cervical spine MRI: comparison with 3T MRI without deep learning

- reconstruction. *Neuroradiology*. 2022;64:2077–83. <https://doi.org/10.1007/s00234-022-03024-6>.
29. Tajima T, Akai H, Yasaka K, et al. Usefulness of deep learning-based noise reduction for 1.5 T MRI brain images. *Clin Radiol*. 2023;78:e13–21. <https://doi.org/10.1016/j.crad.2022.08.127>.
 30. Mandrekar JN. Measures of Interrater Agreement. *J Thorac Oncol*. 2011;6(1):6–7. <https://doi.org/10.1097/jto.0b013e318200f983>.
 31. Kanda Y. Investigation of the freely-available easy-to-use software “EZR” (Easy R) for medical statistics. *Bone Marrow Transplant*. 2013;48:452–8. <https://doi.org/10.1038/bmt.2012.244>.
 32. Zhang J, Tian W-Z, Hu C-H, et al. Age-related changes of normal prostate: evaluation by MR diffusion tensor imaging. *Int J Clin Exp Med*. 2015;8(7):11220–4.
 33. Bura V, Caglic I, Snoj Z, et al. MRI features of the normal prostatic peripheral zone: the relationship between age and signal heterogeneity on T2WI, DWI, and DCE sequences. *Eur Radiol*. 2021;31:4908–17. <https://doi.org/10.1007/s00330-020-07545-7>.

Publisher's Note Springer Nature remains neutral with regard to jurisdictional claims in published maps and institutional affiliations.

Springer Nature or its licensor (e.g. a society or other partner) holds exclusive rights to this article under a publishing agreement with the author(s) or other rightsholder(s); author self-archiving of the accepted manuscript version of this article is solely governed by the terms of such publishing agreement and applicable law.